Report

SOURCE DATA | TRANSPARENT PROCESS | OPEN ACCESS

EMBO reports

Hyperosmotic stress induces 2-cell-like cells through ROS and ATR signaling

Antoine Canat[1], Derya Atilla[1] & Maria-Elena Torres-Padilla[1,2,*]

Abstract

Mouse embryonic stem cells (ESCs) display pluripotency features characteristic of the inner cell mass of the blastocyst. Mouse embryonic stem cell cultures are highly heterogeneous and include a rare population of cells, which recapitulate characteristics of the 2-cell embryo, referred to as 2-cell-like cells (2CLCs). Whether and how ESC and 2CLC respond to environmental cues has not been fully elucidated. Here, we investigate the impact of mechanical stress on the reprogramming of ESC to 2CLC. We show that hyperosmotic stress induces 2CLC and that this induction can occur even after a recovery time from hyperosmotic stress, suggesting a memory response. Hyperosmotic stress in ESCs leads to accumulation of reactive-oxygen species (ROS) and ATR checkpoint activation. Importantly, preventing either elevated ROS levels or ATR activation impairs hyperosmotic-mediated 2CLC induction. We further show that ROS generation and the ATR checkpoint act within the same molecular pathway in response to hyperosmotic stress to induce 2CLCs. Altogether, these results shed light on the response of ESC to mechanical stress and on our understanding of 2CLC reprogramming.

Keywords 2-cell-like cells; hyperosmotic stress; pluripotency; reprogramming; totipotency

Subject Categories Stem Cells & Regenerative Medicine

DOI 10.15252/embr.202256194 | Received 27 September 2022 | Revised 25 June 2023 | Accepted 28 June 2023 | Published online 11 July 2023

EMBO Reports (2023) 24: e56194

Introduction

Mouse embryonic stem cells (ESC) derive from the inner cell mass (ICM) of the blastocyst. Like the ICM, the majority of ESCs in culture are pluripotent, which refers to the capacity to differentiate into all embryonic cell types including the germline (Riveiro & Brickman, 2020). However, a small population of ESCs of around 0.2–0.4% more closely resemble the 2-cell stage embryo and are thus referred to as 2-cell-like cells (2CLC). Two-cell-like cells can arise spontaneously in culture and they exhibit molecular features of totipotent 2-cell stage blastomeres, including high expression of MERVL retrotransposons and the transcription factors *Zscan4* and *Dux*. 2CLCs also display higher plasticity and increased reprogrammability compared with ESCs (Macfarlan *et al*, 2011; Ishiuchi *et al*, 2015).

Multiple molecular pathways that regulate reprogramming from ESCs into 2CLCs have been identified in the last decade (Genet & Torres-Padilla, 2020; Malik & Wang, 2022). These include chromatin regulation and DNA replication, such as changes in DNA replication fork speed, polycomb repressive complex 1.6 (PRC1.6), and chromatin assembly factor-1 (CAF-1) and also spliceosome activity and signaling pathways such as retinoic acid signaling (Ishiuchi *et al*, 2015; Rodriguez-Terrones *et al*, 2018; Fu *et al*, 2019; Wu *et al*, 2020; Iturbide *et al*, 2021; Shen *et al*, 2021; Nakatani *et al*, 2022). Interestingly, none of these pathways can induce the conversion of the whole ESC population into 2CLCs. While this is a common phenomenon in reprogramming models, this also suggests the existence of multiple pathways that safe-guard ESC identity and points toward the importance of discovering additional pathways that can reprogram 2CLCs.

How and whether environmental signals such as mechanical forces regulate changes in cell fate remains an important question currently under intense investigation. Indeed, in a physiological context, cells are under constant pressure from other cells and the environment itself (Dupont & Wickström, 2022). In the skin, which is subject to constant mechanical stress, mechanical changes trigger differentiation of the basal stem cells (Miroshnikova *et al*, 2018). Likewise, ESCs undergo changes in their shape upon exit from naïve pluripotency (Chalut & Paluch, 2016). Such changes are driven by a reduction in membrane tension leading to increased signaling activity by ERK, which is necessary to exit pluripotency (De Belly *et al*, 2021). Accordingly, experimental alteration of forces exerted onto cells can affect cell fate and pluripotency maintenance through global changes in gene expression (Le *et al*, 2016). One type of mechanical pressure is the exposure of cells to hyperosmotic medium. Osmotic stresses affect ionic intake, but they have also been reported to recapitulate some properties of mechanical stress such as deformation of cell membrane and activation of the YAP pathway (Hong *et al*, 2017; Fan *et al*, 2021).

At the molecular level, and in addition to changes in the activity of chromatin-modifying complexes, hyperosmotic stress can lead to elevated levels of reactive-oxygen species (ROS) (Zhang *et al*, 2004;

1 Institute of Epigenetics and Stem Cells (IES), Helmholtz Zentrum München, München, Germany
2 Faculty of Biology, Ludwig-Maximilians Universität, München, Germany
*Corresponding author. Tel: +49 89 3187 3317; E-mail: torres-padilla@helmholtz-muenchen.de

Aquilano *et al*, 2007). Reactive-oxygen species are reactive oxygen-containing small molecules, which are by-products of aerobic respiration and are thus linked to the metabolic state of the cell. Interestingly, 2CLCs contain lower ROS levels compared with ESCs (Rodriguez-Terrones *et al*, 2020). Excessive ROS can be detrimental for the cell by inducing DNA damage for example, which is accompanied by the activation of the DNA Damage Response (DDR) and the checkpoint kinase ATR (ataxia telangiectasia and Rad3 related; Srinivas *et al*, 2019). DNA damage can also lead to the expression of the 2CLC transcription factor DUX through the action of p53 (Storm *et al*, 2014; Grow *et al*, 2021) and both DDR kinases ATR and ATM (ataxia telangiectasia mutated) are required for DNA-damage-induced 2CLCs (Grow *et al*, 2021). Thus, checkpoint activation and DNA damage can induce 2CLCs (Atashpaz *et al*, 2020; Grow *et al*, 2021), but 2CLC can also emerge without checkpoint activation (Zhu *et al*, 2021; Nakatani *et al*, 2022).

Although several studies have investigated the role of mechanical forces during the exit from pluripotency, whether the transition toward a 2CLC fate is regulated by mechanical forces remains unknown. Here, we investigated whether mechanical pressure regulates 2CLC induction by focusing specifically on hyperosmotic stress. We report a new mechanism whereby hyperosmotic stress enhances induction of 2CLCs. We show that hyperosmotic stress in ESCs increases cellular ROS levels and ATR checkpoint activation. Molecularly, we demonstrate that increased ROS levels and ATR checkpoint activation are both involved in in hyperosmotic-mediated 2CLC induction.

Results and Discussion

To monitor 2CLCs, we used a previously described cell line carrying a stable insertion of tbGFP-reporter under the control of the MERVL-LTR sequence, which faithfully recapitulates endogenous MERVL expression and the "2C" transcriptional program (Fig 1A; Macfarlan *et al*, 2012; Rodriguez-Terrones *et al*, 2018). We and others have characterized multiple factors regulating the transition from an ESC to a 2CLC fate, including CAF-1, PRC1.6, miR-34A and miR-344, the transcription factors Dux and p53, but also signaling pathways such as Retinoic Acid signaling and SUMOylation as well as the addition of metabolites to the culture medium (Ishiuchi *et al*, 2015; Rodriguez-Terrones *et al*, 2018, 2020; Iturbide *et al*, 2021; Shen *et al*, 2021; Nakatani *et al*, 2022; Yang *et al*, 2022). Considering the increasing evidence that external mechanical forces can regulate chromatin organization and transcription, leading to eventual changes in cell fate (Le *et al*, 2016; Nava *et al*, 2020), we investigated whether mechanical pressure can regulate 2CLC reprogramming.

Multiple approaches to experimentally modify mechanical pressure can be used in cell culture and include for example plate coating to alter cell attachment, physical compression or a change in osmotic pressure in the medium. Because mouse preimplantation embryos are not yet attached to the uterine wall, making them unlikely to undergo attachment or compression changes, we chose to assess the impact of hyperosmotic stress on 2CLC emergence as osmolarity sensor proteins are expressed throughout preimplantation development (Fong *et al*, 2007). We treated ESCs with several chemicals known to inflict osmotic pressure including sorbitol, Polyethylene glycol (PEG300), or NaCl (Uhlik *et al*, 2003; Arsenijevic *et al*, 2013; Peña-Oyarzun *et al*, 2017; Fan *et al*, 2021; Taïeb *et al*, 2021; Watanabe *et al*, 2021). Treatment of ESCs with 0.2 M sorbitol, 100 mM NaCl or 5% of PEG300 for 24 h strongly induced 2CLCs as measured by FACS (Fig 1B). The effect of sorbitol, NaCl, and PEG300 on 2CLC induction ranged from 7.9- to 16.8-fold compared with the steady-state percentage of 2CLCs in the control, untreated ESCs (Fig 1B). Exposure to each of the compounds: 0.2 M sorbitol, 5% PEG300 and to NaCl at 100 mM, is known to generate a pressure of approximately 500 mOsm kg^{-1}, which is higher than the 300 mOsm kg^{-1} commonly experienced by cells in culture (Arsenijevic *et al*, 2013; Fan *et al*, 2021; Taïeb *et al*, 2021; Watanabe *et al*, 2021). We did not observe cell death under these experimental conditions; however, higher concentrations of sorbitol or NaCl treatment led to increased cell death and we therefore refrained from using those in this study. Mouse embryonic stem cells treated with any of the three hyperosmotic agents displayed altered morphology with more rounded colonies (Fig EV1A). When we applied lower osmotic pressure, by reducing either the sorbitol or NaCl concentration, we did not observe significant changes in 2CLC, suggesting that a minimum amount of osmotic pressure is required to activate downstream molecular changes that result in 2CLC fate conversion (Fig EV1B and C). We reproduced our observation that sorbitol induces 2CLCs in another ESC line carrying a MERVL-tdTomato-reporter, previously described by another group (Macfarlan *et al*, 2012; Fig EV1D).

Figure 1. Hyperosmotic stress induces 2CLCs.

A Experimental design. Top. Reporter cell line used for all experiments carrying a tbGFP-PEST reporter driven by MERVL-LTR. Rare population of cells expressing MERVL become green. Bottom. Example of FACS data sorting ESCs according to tbGFP expression.

B–D Percentage of 2-cell-like cells obtained after hyperosmotic treatments for 24 h (B) or the indicated time (C-D). Shown are the mean ± s.d. from at least two replicates. Individual dots indicate measurement of an independent biological replicate by FACS. Unpaired two-tailed *t*-tests were performed.

E Experimental design. ESC are sorted according to tbGFP fluorescence before sorbitol treatment (t0), after 6 h of sorbitol (t6), or after 24 h of sorbitol treatment (t24). For each collection time, $tbGFP^-$ and $tbGFP^+$ cells are collected and processed for RNA-sequencing.

F MA plots displaying differentially expressed genes in $tbGFP^+$ compared to $tbGFP^-$ cells for the indicated time points following sorbitol treatment, as indicated in E (t0, t6, and t24). $n = 2$ cell cultures in experiments performed on different days. Significantly DE genes are highlighted in red for upregulated transcripts and blue for downregulated transcripts ($P.adj < 0.05$; $Log_2FoldChange(tbGFP^+/tbGFP^-) > 1$ or < -1).

G Heatmap depicting Log2FoldChange of 25 selected 2CLC markers. All genes displayed significative differential expression at t0, t6 and t24 sorbitol treatment in $tbGFP^+$ cells compared to $tbGFP^-$ cells of related time point ($P.adj < 0.01$).

H, I Protein levels assessed by Western blotting in the indicated conditions. Shown is one representative image from two independent replicates.

Data information: Stars indicate significant differences obtained using indicated statistical tests with *$P < 0.05$; **$P < 0.01$; ***$P < 0.001$; ****$P < 0.0001$.
Source data are available online for this figure.

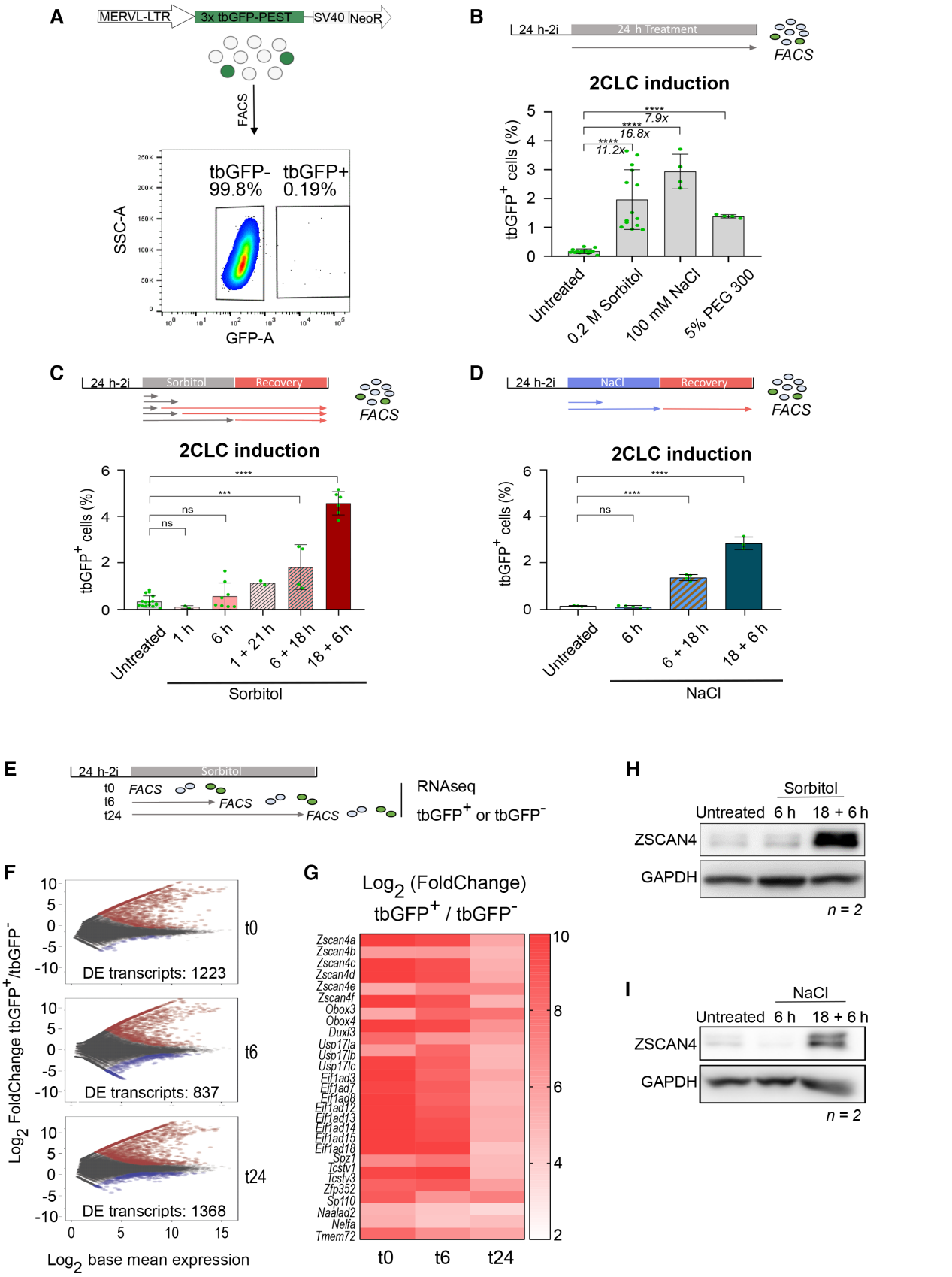
A
MERVL-LTR
3x tbGFP-PEST
SV40
NeoR
FACS
tbGFP- 99.8%
tbGFP+ 0.19%
SSC-A
GFP-A
B
24 h-2i
24 h Treatment
FACS
2CLC induction
tbGFP+ cells (%)
7.9x
16.8x
11.2x
Untreated
0.2 M Sorbitol
100 mM NaCl
5% PEG 300
C
24 h-2i
Sorbitol
Recovery
FACS
2CLC induction
tbGFP+ cells (%)
ns
ns
Untreated
1 h
6 h
1 + 21 h
6 + 18 h
18 + 6 h
Sorbitol
D
24 h-2i
NaCl
Recovery
FACS
2CLC induction
tbGFP+ cells (%)
ns
Untreated
6 h
6 + 18 h
18 + 6 h
NaCl
E
24 h-2i
Sorbitol
t0
t6
t24
FACS
RNAseq
tbGFP+ or tbGFP-
F
Log2 FoldChange tbGFP+/tbGFP-
DE transcripts: 1223
DE transcripts: 837
DE transcripts: 1368
t0
t6
t24
Log2 base mean expression
G
Log2 (FoldChange)
tbGFP+ / tbGFP-
Zscan4a
Zscan4b
Zscan4c
Zscan4d
Zscan4e
Zscan4f
Obox3
Obox4
Duxf3
Usp17la
Usp17lb
Usp17lc
Eif1ad3
Eif1ad7
Eif1ad8
Eif1ad12
Eif1ad13
Eif1ad14
Eif1ad15
Eif1ad18
Spz1
Tcstv1
Tcstv3
Zfp352
Sp110
Naalad2
Nelfa
Tmem72
t0
t6
t24
H
Sorbitol
Untreated
6 h
18 + 6 h
ZSCAN4
GAPDH
n = 2
I
NaCl
Untreated
6 h
18 + 6 h
ZSCAN4
GAPDH
n = 2

Figure 1.

In human cells, osmotic changes rapidly modify cell morphology and can activate signaling pathways within seconds to minutes following hyperosmotic stress (Cai *et al*, 2019). Therefore, we next investigated the time-window during which osmotic pressure induces 2CLC emergence. For this, we treated ESC with 0.2 M sorbitol for different time periods and assessed the percentage of 2CLCs. Addition of sorbitol for 1 or 6 h did not affect the percentage of 2CLCs (Fig 1C). This could be due, at least in part, to the time required to transcribe, translate, and fold the tbGFP reporter. However, because osmotic changes are reversible, we tested whether a recovery time would enable tbGFP detection. Indeed, when we measured the percentage of 2CLCs 22 h after only 1 h sorbitol treatment (1 h + 21 h), we observed a robust increase in 2CLCs (Fig 1C). 2CLC-induction was higher when sorbitol treatment lasted for at least 6 h with 18 h recovery (6 + 18 h) and we observed greatest induction upon 18 h of treatment with 6 h recovery (18 h + 6 h; Fig 1C). These results suggest that while sorbitol elicits a fast response, the emergence of 2CLCs may rather stem from downstream transcriptional changes arising upon hyperosmotic stress. Interestingly, we noted that 18 h sorbitol treatment followed by 6 h recovery time led to a higher conversion of 2CLCs compared with a 24 h of continuous sorbitol treatment (Fig 1C). This may be due to adaptation of ESCs to osmotic pressure over a longer period of exposure or, alternatively, to desensitization. Because 24 h exposure to 100 mM NaCl strongly induced 2CLCs (Fig 1B), we also assessed whether a short exposure to NaCl followed by a recovery period can induce 2CLCs, similarly to our findings with sorbitol. Of note, culturing ESCs under NaCl 100 mM for only 6 h did not increase the amount of 2CLCs as for sorbitol (Fig 1D). However, exposure to 100 mM NaCl for 6 or 18 h followed by a recovery time of 18 or 6 h after washing-out NaCl from the medium, respectively, led to a strong induction of 2CLCs (Fig 1D), suggesting that similar kinetics of 2CLC induction occur in response to hyperosmotic stress regardless of the stimulus. Nevertheless, the range of 2CLC induction upon culturing in the presence of 100 mM NaCl for at least 18 h is similar with or without a recovery period (Fig 1D). Overall, these data demonstrate that osmotic stress in ESCs, specifically through applying hyperosmotic pressure, leads to 2CLC reprogramming. In addition, a short stress is sufficient to elicit 2CLC induction when allowing for a recovery period, indicating a fast-acting mechanism at the cellular level that then persists beyond the osmotic shock.

We next addressed whether hyperosmotic stress induces the endogenous "2C" transcriptional programme beyond our 2C:: reporter by performing RNA-seq. We sorted cells based on tbGFP content before (t0) and after 6 (t6) or 24 (t24) hours of sorbitol treatment (Fig 1E) and performed differential gene expression (DE) analysis of $tbGFP^+$ cells compared with $tbGFP^-$ cells at each of the three time points (Fig 1F). MA plots indicated a large transcriptional change of $tbGFP^+$ cells already after 6 h of sorbitol treatment, compared with tbGFP- cells (Fig 1F). These changes were similar to those observed after 24 h (837 and 1,368 DE genes at t6 and at t24, respectively; *P*-value < 0.05; Dataset EV1). Indeed, the number of DE genes between control cells and the 24 h-treated $tbGFP^+$ cells was only slightly smaller than the number of DE genes after 6 h sorbitol treatment (215 and 351 genes, respectively) (Fig EV1E and F; Table EV1). In addition, and in line with earlier reports, we observed more upregulated genes than downregulated genes (Fig 1F; Dataset EV1) (Ishiuchi *et al*, 2015). Importantly, differentially expressed genes included well-described 2CLC markers such as the *Zscan4* cluster, the transcription factors *Dux*, *Zfp352* and *Spz1*, or the *Obox*-family, *Nelfa*, *Naalad2*, and *Eif1ad* genes, which all displayed strong transcriptional upregulation (*P*-value < 0.01, Log2FC > 2) (Figs 1G and EV1E). We note that 6 h-treated $tbGFP^-$ cells displayed slightly increased expression of most of these 2CLC markers, including *Zscan4* (Fig EV1E; Dataset EV1). While this results in an apparent fold decrease of *Zscan4* in the 24 h-treated tbGFP+ cells compared to t0 (Fig 1G), the raw counts confirm an absolute increase in the expression of 2CLC markers at the 24 h timepoint (Dataset EV1). Importantly, our observations that *Zscan4* is already upregulated in the $tbGFP^-$ cell population (e.g. MERVL negative) after 6 h sorbitol treatment strengthen our conclusion that ESCs are already transitioning towards the 2CLC state at this time point as they have activated *Zscan4* but not yet MERVL (Rodriguez-Terrones *et al*, 2018). We confirmed changes in expression of selected 2CLC-markers using RT-qPCR experiments. Indeed, we observed higher expression levels of *Dux*, *MERVL*, and *Zscan4* after 18 h treatment of sorbitol or NaCl followed by the 6 h recovery period (Fig EV1H and I). Importantly, hyperosmotic stress applied to other cell type, namely MEFs, did not lead to an increase in the expression of 2CLC markers *Dux* and *Zscan4* (Fig EV1J), suggesting that the hyperosmotic response toward a "2C" fate may be limited to ESCs. We conclude that hyperosmotic stress induces 2CLCs with a genuine "2C" transcriptional programme.

Because we observed the strongest effect on 2CLC induction with sorbitol upon 18 h of hyperosmotic stress followed by a recovery time of 6 h (18 + 6 h), we used these experimental conditions for subsequent experiments. As a comparison, we also focused on the 6 h treatments without recovery, which did not affect 2CLC emergence.

The upregulation of 2CLC-markers was also visible at the protein level, which we confirmed by Western blot for ZSCAN4 in ESCs cultured under the same experimental conditions with sorbitol and NaCl (Fig 1H and I). Interestingly, *Dux* mRNA levels were upregulated already after 6 h of hyperosmotic treatment to similar levels than those after the 6 h + 18 h treatment (Fig EV1G and H). These results indicate that hyperosmotic stress elicits a fast transcriptional response, but additional time is required to induce a broader 2CLC-transcriptional program (Fig 1C and D). These interpretations are in line with work showing that DUX can directly activate *MERVL*, placing MERVL activation downstream of DUX (Hendrickson *et al*, 2017). Interestingly, most of the naturally arising 2CLCs derive from an intermediate ESC population, which express *Zscan4* (Rodriguez-Terrones *et al*, 2018). Because we detect *Dux* expression prior to *Zscan4* expression, our results suggest that stress-induced 2CLCs may not necessarily undergo the same intermediate state and instead may arise as a consequence of direct *Dux* activation. Indeed, DUX activation could bypass the naturally occurring Zscan4+ intermediate cell state by leading to direct and robust activation of MERVL. Likewise, under DNA damage conditions, p53 can directly bind and activate *Dux* expression (Grow *et al*, 2021).

We next investigated the potential mechanism of action whereby hyperosmotic stress leads to 2CLC induction. Hyperosmotic stress leads to changes in oxidative metabolism, notably by generating higher levels of reactive oxygen species (ROS) (Zhang *et al*, 2004; Aquilano *et al*, 2007). Thus, we addressed whether ROS levels are affected in ESCs upon sorbitol treatment. For this, we measured

ROS by incubating ESCs with the CellROX fluorescent probe and quantified fluorescence intensity, as previously described (Rodriguez-Terrones *et al*, 2020). Sorbitol increased the ROS levels as detected by CellROX both after 6 and 18 h of treatment followed by a recovery time, although the increase after only 6 h sorbitol treatment was not statistically significant, suggesting that ROS levels may build over time (Fig 2A). It is interesting to note that, while steady state endogenously arising 2CLCs display lower ROS levels associated with their metabolic changes (Rodriguez-Terrones *et al*, 2020), our results here suggest that a sudden increase in ROS could act as a trigger for 2CLC conversion (Rodriguez-Terrones *et al*, 2020). This is consistent with previous observations indicating that H_2O_2 treatment can increase the proportion of 2CLCs (Zhang *et al*, 2019). To mechanistically assess whether production of ROS is associated with 2CLC induction, we next treated ESCs with the ROS scavenger N-acetyl-cysteine (NAC), which counteracts ROS effects (Zafarullah *et al*, 2003; Zhang *et al*, 2019). First, we confirmed that NAC effectively blocks ROS generation in ESCs (Fig EV2A). Then, to determine whether ROS production is important during the time window spanning sorbitol treatment or during the recovery time, we treated ESCs with NAC either during the first 18 h of sorbitol incubation or during the 6 h of the recovery period. We find that addition of NAC during the sorbitol treatment strongly reduces the emergence of 2CLCs, albeit not completely (Fig 2B). However, addition of NAC during the recovery time does not affect the percentage of 2CLCs (Fig 2B). These results indicate that hyperosmotic stress on ESCs leads to the induction of higher levels of ROS. In addition, our data with the ROS scavenger indicate that hyperosmotic stress-induces 2CLC reprogramming in part through the generation of ROS.

In addition to its known effect on the cell membrane, sorbitol can affect organelle homeostasis and nuclear size (Khavari & Ehrlicher, 2019; Srivastava *et al*, 2021), which could potentially have direct effects on chromatin integrity and/or gene expression. To address whether sorbitol exposure alters nuclear shape in ESCs, we measured nuclear size following sorbitol treatment. In control, untreated ESCs, the average nuclear cross-sectional area is 162μm^2 (Fig EV2B). However, after addition of sorbitol for 6 h nuclei became smaller, with an average cross-sectional area of 132μm^2 (Fig EV2B). The effect of sorbitol on nuclear size was transient and reversible, since nuclear size returned to 152μm^2 after recovery period of 18 h, highlighting the reversible nature of hyperosmotic stress.

Exerting pressure onto the nucleus either through direct physical compression or, in this case through hyperosmotic stress, can lead to accumulation of DNA damage (Zhang *et al*, 2004; Kumar *et al*, 2014; Nava *et al*, 2020; Shah *et al*, 2021). In human cells, the ATR checkpoint is also activated in response to sorbitol treatment (Kumar *et al*, 2014). We thus next assessed whether ESCs display signs of DNA damage after sorbitol treatment. We examined the levels of key DDR effectors by Western blot after 6 h or after 18 h of sorbitol exposure followed by the recovery time. Within 6 h exposure to sorbitol, we observed induction of phosphorylated ATR as well as higher protein levels of CHK1, with a slight increase in phosphorylated CHK1 (Fig 2C). Levels of γ-H2A.X at this time point were variable between replicates (Fig 2C). These data indicate that activation of DDR, including the checkpoint kinase ATR, occurs during the first hours of sorbitol treatment. Phosphorylated ATR continued to increase during the 18 h sorbitol treatment followed by the recovery time, and γ-H2A.X was consistently induced at this time (Fig 2C). However, CHK1 protein levels returned to basal levels after the 18 + 6 h treatment. Thus, sorbitol induces the activity of some of the components of the DDR in ESCs, albeit with distinct kinetics.

To better understand the potential role of ATR activation in 2CLC emergence upon hyperosmotic stress, we used the ATR inhibitor BAY-1895344. We confirmed that the BAY-1895344 inhibitor efficiently reduces ATR phosphorylation and its downstream target, CHK1, by incubating ESCs with 2 mM hydroxy-urea (HU) in the presence and absence of BAY-1895344 (Fig EV2C and D). We then treated ESCs with or without ATR inhibitor either during the hyperosmotic stress itself or during the recovery time, after which we assessed the number of 2CLCs (Fig 2D). Inhibition of ATR activity at the same time as the sorbitol treatment strongly reduced the amount of induced 2CLCs, which was decreased by more than three-fold, suggesting that ATR pathway activation is involved in 2CLC reprogramming in response to sorbitol (Fig 2D). In contrast, inhibiting ATR during the recovery period only partly decreased 2CLC induction (~ 1.5-fold; Fig 2D). These results are similar to our observations using the ROS scavenger NAC, namely that ROS scavenger treatment reduces sorbitol-induced 2CLC emergence primarily during the osmotic shock (Fig 2B). However, contrary to what we observe for ATR inhibition, NAC treatment during the recovery time had no effect on 2CLC induction, suggesting that ROS is important for 2CLC induction during the first hours of hyperosmotic shock, whereas ATR may continue to signal after the shock. Importantly, inhibition of ATR activity also strongly impaired the capacity of 100 mM NaCl to induce 2CLCs (Fig 2D). These results indicate that ATR checkpoint activation is required—at least partially—for hyperosmotic-mediated reprogramming of 2CLCs. However, this effect is not complete, suggesting that additional pathways contribute to 2CLC induction upon osmotic stress.

Next, we asked whether ATR activity and ROS generation function together or in separate pathways in their ability to mediate hyperosmotic-stressed induction of 2CLCs by sorbitol. For this, we incubated ESCs with sorbitol for 18 h and added either the ATR inhibitor, the NAC ROS-scavenger or both combined, allowing a subsequent recovery period of 6 h. ATR inhibition and addition of NAC to the culture had a similar effect in reducing sorbitol-induced 2CLCs to about half of the induction effect elicited upon sorbitol treatment (Fig 3A). Interestingly, inhibiting both pathways simultaneously did not completely abolish sorbitol-induced 2CLCs and resulted instead in similar levels of 2CLC induction as in the single treatment (Fig 3A). These results indicate that both ATR-mediated checkpoint activation and ROS production might be acting within the same pathway. To verify this interpretation with another hyperosmotic agent, we performed the same experiment using 100 mM NaCl treatment. Here, we note that ATR inhibition displayed stronger inhibition in NaCl-mediated 2CLC induction, compared with NAC (Fig 3B). However, addition of both, ATR inhibitor and NAC simultaneously to the culture medium did not fully prevent 2CLC-induction upon osmotic stress elicited by 100 mM NaCl (Fig 3B). Previous reports have demonstrated that higher levels of ROS lead to DNA damage and DNA damage signaling (Willis *et al*, 2013; Salehi *et al*, 2018). We noted that the effect of the ROS scavenger in preventing 2CLC induction upon osmotic stress was limited to the time-window of the hyperosmotic stress itself but was no longer observed during the recovery time (Fig 2B). This was in contrast to

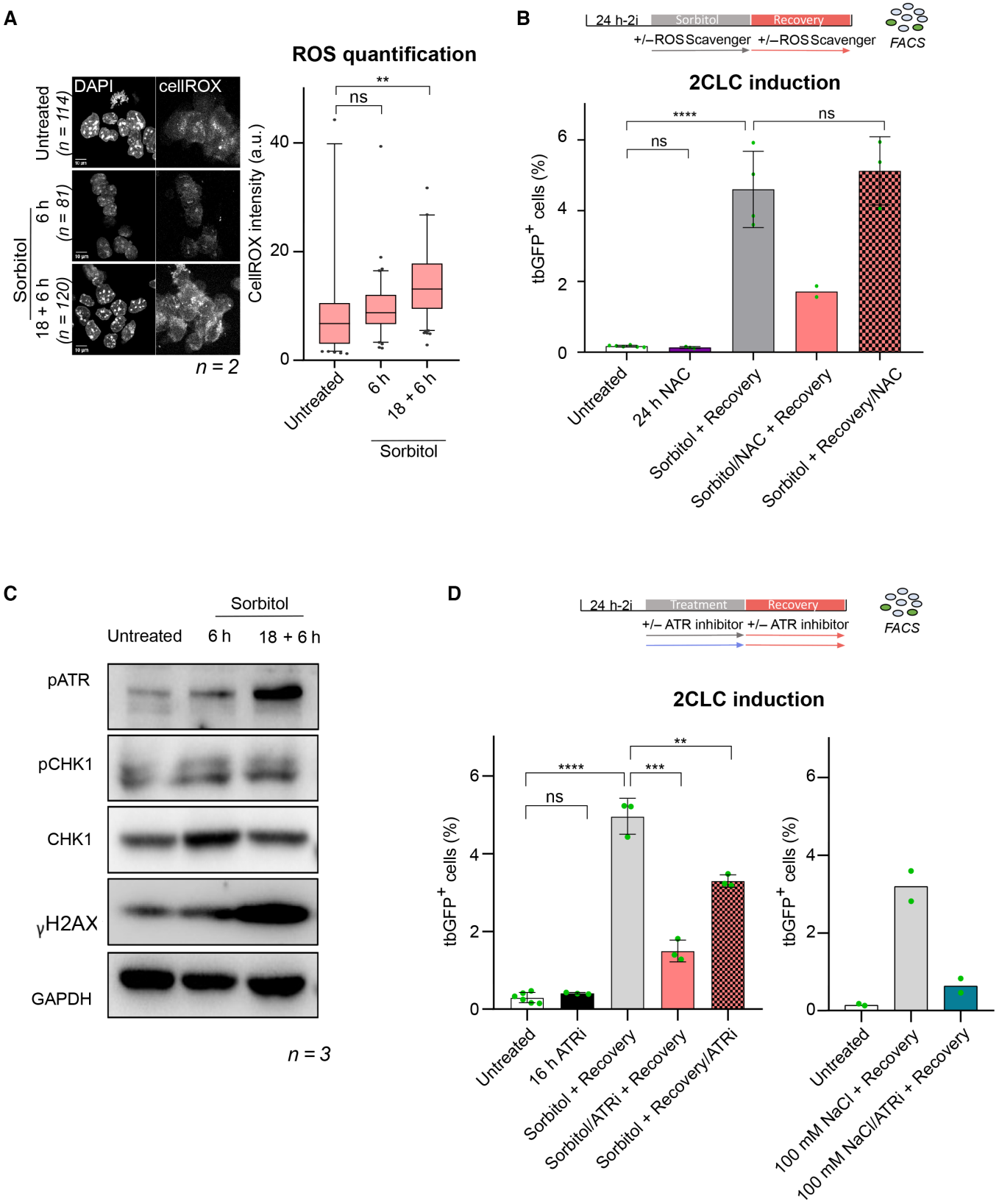

Figure 2.

Figure 2. Hyperosmotic-mediated 2CLC induction is mediated through ROS generation and ATR activation.

A (Left) Representative single confocal z-section of CellROX-DeepRed fluorescence of ESC treated with 0.2 M sorbitol for the indicated time from two biological replicates. Scale bar: 10 μm. (Right) Quantification of CellROX-DeepRed fluorescence intensity from single z-sections from two biological replicates. Two-tailed Mann–Whitney tests were performed. Boxes indicate the range between the first and third quartile, the line indicates the median and the whiskers display the spread from 5 to 95% of the data.

B Percentage of 2CLCs obtained by FACS after the indicated sorbitol treatment with addition of ROS scavenger N-AcetylCysteine (NAC) during either the sorbitol treatment or recovery time. Shown are the mean ± s.d. from at least two replicates. Individual dots indicate measurement of an independent biological replicate by FACS. Unpaired two-tailed *t*-tests were performed.

C Protein levels assessed by Western blotting in the indicated conditions. Shown is one representative image from three independent replicates.

D Percentage of 2CLCs obtained by FACS after the indicated hyperosmotic treatment with addition of ATR inhibitor during either the hyperosmotic stress or recovery time. Shown are the mean ± s.d. from at least two replicates. Individual dots indicate measurement of an independent biological replicate by FACS. Same untreated dots are shown. Two-tail *t*-tests were performed.

Data information: Stars indicate significant differences obtained using indicated statistical tests with *$P < 0.05$; **$P < 0.01$; ***$P < 0.001$; ****$P < 0.0001$.
Source data are available online for this figure.

ATR inhibition, which affected 2CLC emergence mediated by hyperosmotic stress throughout the whole time of the experimental setting (Fig 2D). Considering that dampening ROS and inhibiting ATR together does not result in a stronger reduction in 2CLC emergence compared to any of these two alone, we propose that ROS would be produced first upon hyperosmotic stress, leading to subsequent activation of the ATR checkpoint.

Several molecular pathways have been documented to induce 2CLCs in ESC cultures (Genet & Torres-Padilla, 2020; Iturbide & Torres-Padilla, 2020; Malik & Wang, 2022). While these pathways seem to be rather broad, ranging from chromatin regulation to osmotic stress, it is important to note that the efficiency at which 2CLC conversion is achieved varies considerably. In terms of signaling, 2CLCs can be induced, for example, by changing the metabolite supply in the culture medium with sodium acetate (Rodriguez-Terrones *et al*, 2020), but also through low concentrations of retinoic acid (Tagliaferri *et al*, 2020; Iturbide *et al*, 2021; Wang *et al*, 2021) and mechanical stress through osmolarity modulation (this work). To better understand whether these signaling pathways act conjointly or independently, we next incubated ESCs with combinations of sodium acetate, retinoic acid, and sorbitol and determined the percentage of 2CLCs by FACS. We also included the spliceosome inhibitor Pladienolide B, since downregulation or chemical inhibition of spliceosome activity can induce 2CLCs (Rodriguez-Terrones *et al*, 2018; Shen *et al*, 2021). After 24 h treatment, we observed that independently, sorbitol, sodium acetate, and retinoic acid increase 2CLCs to a similar level (Fig 3C). Treatment with the spliceosome inhibitor Planieloide B had a stronger effect, with the ESC population containing up to 8% of 2CLCs (Fig 3C). Interestingly, addition of sorbitol together with any of the other 2CLC inducers led to a significant cumulative increase in the percentage of 2CLCs compared with sorbitol alone (Fig 3C). We observed the strongest synergistic effect in 2CLC conversion when we combined retinoic acid and sorbitol in the culture medium, which together induced 2CLC emergence to ~ 25% of ESC population (Fig 3C). These results suggest that hyperosmotic stress or signaling mediated by retinoic acid may sensitize ESCs, rendering them more prone for 2CLC emergence and addition of both greatly increase the reprogramming events.

How cells can sense environmental stress and whether and how stress can lead to changes in cell fate is currently an exciting question in the stem cell and developmental biology fields. While it is known that early mouse embryos are particularly sensitive to changes in osmolarity, this area remains understudied (Wang *et al*, 2011; Zhang *et al*, 2012). Our work indicates that ESCs respond to changes in osmotic pressure by generating ROS and activating ATR and that these can lead to changes in cell fate (Fig 3D). However, it remains to be determined whether hyperosmotic shock also affects differentiation pathway toward embryonic or extraembryonic lineages. Interestingly, this pathway can elicit a synergistic effect with other signaling pathways known to induce 2CLCs. While ATR has been involved in mediating 2CLC induction under conditions of genotoxic stress (Atashpaz *et al*, 2020; Grow *et al*, 2021), ATR activation is dispensable for naturally arising 2CLCs emerging spontaneously in culture (Nakatani *et al*, 2022). It would be important to determine whether the pathways leading to 2CLC activation under stress conditions, such as the work we describe here, are also in play in naturally cycling 2CLCs and how they link to the molecular features characteristic of 2CLCs, including for example slow DNA replication fork speed (Nakatani *et al*, 2022). Additionally, the interplay between ROS and ATR activation in ESC

Figure 3. ROS generation and ATR activation act within the same molecular pathway in response to hyperosmotic stress.

A Percentage of 2CLCs obtained by FACS after the indicated sorbitol treatment with addition of ROS scavenger N-AcetylCysteine (NAC) or ATR inhibitor. Shown are the mean ± s.d. from five replicates. Individual dots indicate measurement of an independent biological replicate by FACS. Unpaired two-tailed *t*-tests were performed.

B Percentage of 2CLCs obtained by FACS after the indicated NaCl treatment with the addition of ROS scavenger N-AcetylCysteine (NAC) or ATR inhibitor. Shown are the mean ± s.d. from at least two replicates. Individual dots indicate measurement of an independent biological replicate by FACS. Unpaired two-tailed *t*-tests were performed.

C Percentage of 2CLCs obtained by FACS after the indicated treatments. Shown are the mean ± s.d. from at least two replicates. Individual dots indicate measurement of an independent biological replicate by FACS. Individual and combinatorial treatments performed with 0.2 M of sorbitol, 24 mM of sodium acetate, 2.5 nM of PlaB spliceosome inhibitor and 0.53 μM of retinoic acid. Unpaired two-tailed *t*-tests were performed. Unpaired two-tailed *t*-tests were performed against each individual treatment in the combinatorial experiments.

D Proposed model of action of hyperosmotic-mediated induction of 2CLCs.

Data information: Stars indicate significant differences obtained using indicated statistical tests with *$P < 0.05$; **$P < 0.01$; ***$P < 0.001$; ****$P < 0.0001$.
Source data are available online for this figure.

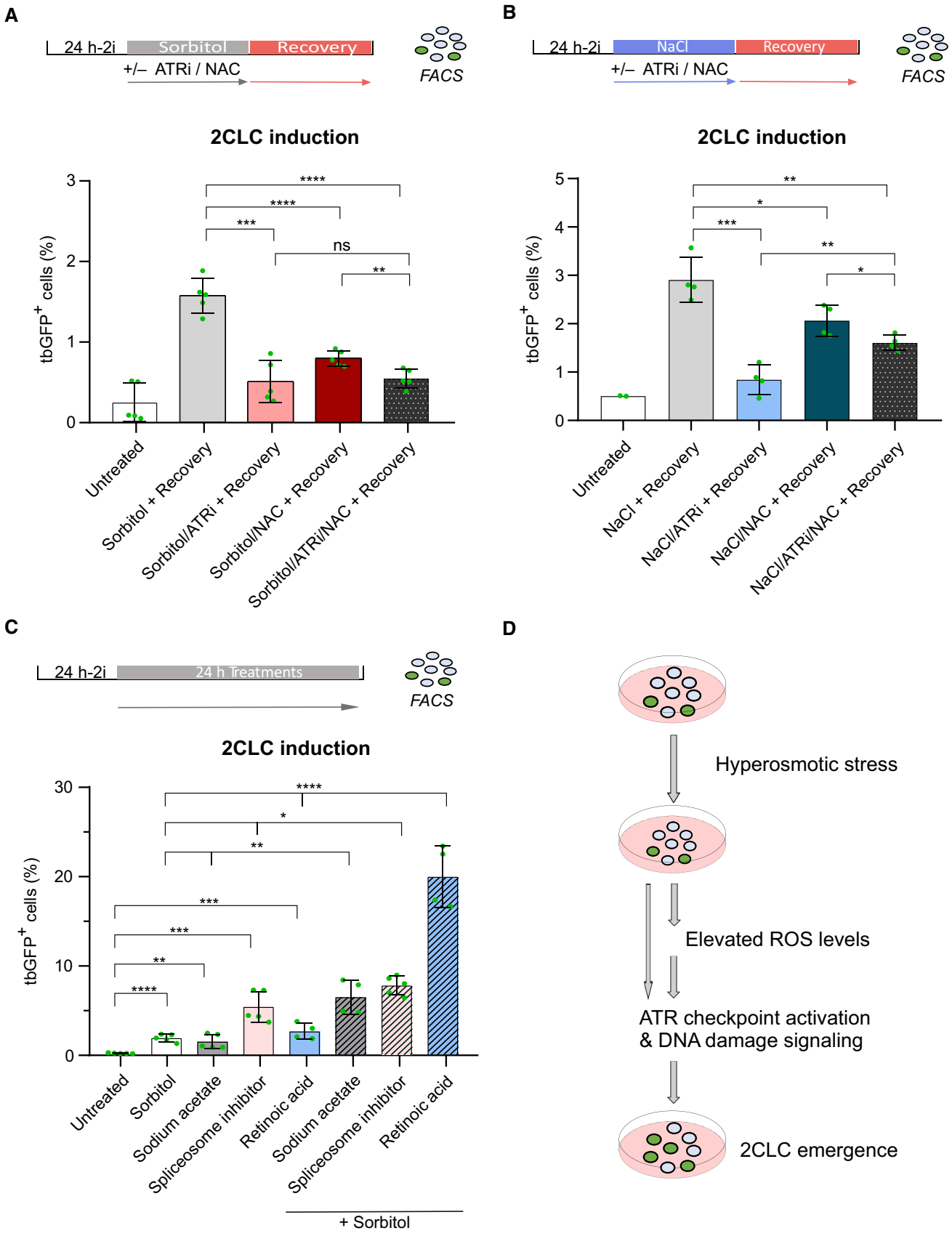

Figure 3.

remains to be fully investigated. It is possible that ROS production, which occurs primarily through mitochondrial activity, may be linked to the different shapes of mitochondria that have been observed in 2CLCs and which differ to mitochondria in ESCs (Rodriguez-Terrones *et al*, 2020). We speculate that a sudden hyperosmotic stress could favor this transformation of mitochondria morphology. Furthermore, because elevated levels of ROS can also generate oxidative damage, notably by increasing 8-oxoguanine, it remains to be explored whether 8-oxoguanine and base-excision repair pathways are implicated in 2CLC emergence. Altogether, our work sheds light into the response of mouse ESCs to mechanical stress and the interaction of hyperosmotic stress with multiple molecular pathways in 2CLC conversion.

Materials and Methods

Cell culture

Mouse E14 embryonic stem cells carrying the 2C: tbGFP-PEST reporter were established and characterized previously (Nakatani *et al*, 2022). Cells were grown in Dulbecco's modified Eagles's medium (DMEM) with Glutamax (Gibco) containing 15% ES-certified fetal calf serum (Gibco), 2X leukemia inhibitory factor (LIF), 0.05 mM 2-betamercaptoethanol (Gibco), 0.1 mM nonessential amino acids (Gibco), 100 units/mL penicillin and streptomycin (Gibco) and cultured on gelatin-coated plates. For expansion, medium was supplemented with 3 μM CHIR99021 and 1 μM PD0325901. For all experiments, cells were passaged and plated without the two inhibitors. All chemicals used were added after 24 h of 2i withdrawal. Thus, all the experiments were to have a consistent readout of 2CLCs after 48 h upon 2i withdrawal as this time point has been previously used to quantify optimal 2CLC induction (Rodriguez-Terrones *et al*, 2018; Iturbide *et al*, 2021). The medium was changed every day and cells passaged every 2 days. Sorbitol was prepared and kept at 4°C from powder (SIGMA) and used at 0.2 M unless indicated differently. Sodium chloride was prepared and kept at 4°C from powder (SIGMA) and added to the medium at 100 mM unless otherwise stated. PEG300 was prepared from powder (SIGMA) and kept at 4°C. Sodium acetate was prepared and kept at 4°C from powder and used at 24 mM like previously reported (Rodriguez-Terrones *et al*, 2020). ATR inhibitor BAY-1895344 was added at 0.1 μM (Biomol). N-acetyl-cysteine was prepared fresh before each experiment from powder and used at 1 mM (SIGMA). Retinoic acid was used at 0.53 μM as previously described (Iturbide *et al*, 2021). Pladienolide B was used at 2.5 nM as previously described (Shen *et al*, 2021). Primary MEFs were thawed and cultured for 3 days before hyperosmotic treatment in DMEM with Glutamax (Gibco) containing 15% ES-certified fetal calf serum (Gibco), 0.05 mM 2-betamercaptoethanol (Gibco), 0.1 mM non-essential amino acids (Gibco), 100 units/ml penicillin and streptomycin (Gibco) on gelatin-coated plates.

Fluorescence-assisted cell sorting (FACS)

After collection of ESCs using 0.25% trypsin, cells were resuspended in ESC medium and kept on ice before FAC-sorting. Calculation of 2CLC population was based on tbGFP expression after exclusion of dead and doublet cells using forward and side-scatter profiles. Sorting was performed on a FACS Melody (BD Biosciences). Recording of the data was done using the FACS Chorus software before processing using the FlowJo software.

Real-time RT-qPCR

Total RNA was extracted from ESCs using Trizol followed by chloroform purification (SIGMA). RNA extracts were treated with turbo DNAse for 1 h (ThermoFisher Scientific) to remove genomic DNA. Reverse transcription was performed with Go Script (Promega) with both random hexamers and oligodT oligos using 1 μg total RNA. Real-time PCR was performed with SYBR Green master mix (Promega) on a LightCycler 96 Real-time PCR system (Roche). The list of primers used for qPCR is indicated in Table EV2.

RNA-sequencing and analysis

After 48 h of culture and the indicated sorbitol treatment (6 or 24 h), 50,000 cells were FACS sorted into tbGFP- and tbGFP^{+}. Total RNA was extracted using PicoPure RNA Isolation Kit (ThermoFisher Scientific). RNA samples were treated with turbo DNAse (Life Technologies). Two biological replicates were collected for each sample. Libraries were prepared with a TruSeq Stranded Gold Total RNA Library Prep Human/Mouse/Rat (Illumina) and IDT for Illumina TruSeq RNA Indexes (Illumina) according to the manufacturer's protocol. Excess primers were removed through purification using AMPure XP beads (Agencourt Biosciences Corporation). The quality of the libraries was verified with a 2,100 Bioanalyzer using High Sensitivity DNA kit (Agilent). Sequencing was performed on an Illumina NovaSeq sequencer (Illumina) using a 150-bp paired-end protocol following the Illumina's instructions. Data were mapped to the reference mouse genome (mm10) using HiSAT2 with default options for paired library. Read counts were measured using FeatureCounts with default options for unstranded data using UCSC KnownGene as annotation file. Differential gene expression between conditions was performed using DESeq2 with a prefilter value of 10 and a ratio estimation size factor for all transcripts. FPKM values for all transcripts were computed using Cufflinks package with Cufflinks Effective Length Correction. QC features and mapping statistics are shown in Table EV1. DESeq2 results and FPKM values are shown in Dataset EV1.

ROS measurements

Cells were plated on gelatin-coated 12-mm coverslips for 48 h and the different treatments were performed. CellROX Deep Red reagent (ThermoFisher Scientific) was added to the culture medium according to the manufacturer's recommendations for 30 min. Cells were washed three times with PBS, then fixed with 3% PFA for 15 min and mounted in Vectashield with DAPI (Vector laboratories) before imaging, according to the manufacturer's recommendation.

Immunofluorescence

Cells were plated on gelatin-coated 12-mm coverslips for 48 h. Treatments with 2 mM HU and 2 mM HU + 0.1 μM ATR inhibitor

were performed overnight. Cells were washed with PBS then fixed with 4% PFA. Blocking was made in 3% BSA/PBS for 30 min. Cells were incubated with primary antibody overnight. After washes with PBS, blocking was performed in 3% BSA/PBS for 30 min. Incubation with secondary antibody were done at room temperature for 1 h. Cells were mounted in Vectashield with DAPI (Vector laboratories). The list of antibodies used for immunofluorescence is indicated in Table EV2.

Image acquisition

All image acquisition was performed on an inverted SP8 confocal microscope (Leica) using a 63x oil objective. Image analysis was made using ImageJ. Manual segmentation of ESC nuclei was performed based on the DAPI signal and parameters such as nuclear area and fluorescence intensities were measured using the standard ImageJ plugins. No experiment was performed blindly.

Western blot

Total proteins were extracted using RIPA buffer containing 0.1% SDS and 1% NP40 and protease inhibitor cocktail (Roche). Protein electrophoresis was made in a 10% poly-acrylamide gel transferred on 0.45 µm PVDF membrane activated with methanol (Millipore). Membranes were blocked in 5% milk, 0.1% tween/PBS for 30 min at room temperature for all antibodies except p-ATR and p-CHK1 for which blocking and antibody incubation were done in 3% BSA, 0.1% tween/PBS. Primary antibody incubation was performed overnight at 4°C. After three washed in 0.1% tween/PBS, membranes were incubated with secondary HRP-conjugated antibodies for 1 h at room temperature. Membranes were washed three times in 0.1 tween/PBS and visualized by chemiluminescence using ECL prime (Cytiva). The list of antibodies used for Western blot is listed in Table EV2.

Data visualization and statistical analysis

All histograms and dot plots were generated using using Prism Graphpad v8. MA Plots and heatmaps were generated using base R function. All statistical tests are indicated in figure legends. *P*-values are represented as follow: *< 0.05, **< 0.01, ***< 0.001, ****< 0.0001.

Data availability

RNA-sequencing data generated in this study are available in GEO using the access number GSE231475 (https://www.ncbi.nlm.nih.gov/geo/query/acc.cgi?acc=GSE231475).

Expanded View for this article is available online.

Acknowledgments
Work in the Torres-Padilla laboratory is funded through the Helmholtz Association and the German Research Foundation (DFG) Project-ID 213249687 (SFB 1064). We thank Adam Burton and Tsunetoshi Nakatani for critical reading of the manuscript. Open Access funding enabled and organized by Projekt DEAL.

Author contributions
Antoine Canat: Conceptualization; data curation; formal analysis; investigation; writing – original draft; writing – review and editing. **Derya Atilla:** Investigation. **Maria-Elena Torres-Padilla:** Conceptualization; supervision; funding acquisition; writing – original draft; writing – review and editing.

Disclosure and competing interests statement
The authors declare that they have no conflict of interest.

References

Aquilano K, Filomeni G, di Renzo L, di Vito M, di Stefano C, Salimei PS, Ciriolo MR, Marfé G (2007) Reactive oxygen and nitrogen species are involved in sorbitol-induced apoptosis of human erithroleukaemia cells K562. *Free Radic Res* 41: 452 – 460

Arsenijevic T, Vujovic A, Libert F, De Beeck AO, Hébrant A, Janssens S, Grégoire F, Lefort A, Bolaky N, Perret J *et al* (2013) Hyperosmotic stress induces cell cycle arrest in retinal pigmented epithelial cells. *Cell Death Dis* 4: e662

Atashpaz S, Shams SS, Gonzalez JM, Tripodo C, Cancila V, Bachi A, Ferrari F (2020) ATR expands embryonic stem cell fate potential in response to replication stress. *Elife* 9: 1 – 30

Cai D, Feliciano D, Dong P, Flores E, Gruebele M, Porat-shliom N, Sukenik S, Liu Z, Lippincott-schwartz J (2019) Phase separation of YAP reorganizes genome topology for long-term YAP target gene expression. *Nat Cell Biol* 21: 1578 – 1589

Chalut KJ, Paluch EK (2016) The Actin cortex: a bridge between cell shape and function. *Dev Cell* 38: 571 – 573

De Belly H, Stubb A, Yanagida A, Labouesse C, Jones PH, Paluch EK, Chalut KJ (2021) Membrane tension gates ERK-mediated regulation of pluripotent cell fate. *Cell Stem Cell* 28: 273 – 284.e6

Dupont S, Wickström SA (2022) Mechanical regulation of chromatin and transcription. *Nat Rev Genet* 23: 624 – 643

Fan Y, Zhao H, Feng X (2021) Hypertonic pressure affects the pluripotency and self-renewal of mouse embryonic stem cells. *Stem Cell Res* 56: 102537

Fong B, Watson PH, Watson AJ (2007) Mouse preimplantation embryo responses to culture medium osmolarity include increased expression of CCM2 and p38 MAPK activation. *BMC Dev Biol* 7: 1 – 16

Fu X, Wu X, Djekidel MN, Zhang Y (2019) Myc and Dnmt1 impede the pluripotent to totipotent state transition in embryonic stem cells. *Nat Cell Biol* 21: 835 – 844

Genet M, Torres-Padilla ME (2020) The molecular and cellular features of 2-cell-like cells: a reference guide. *Development* 147: dev189688

Grow EJ, Weaver BD, Smith CM, Guo J, Stein P, Shadle SC, Hendrickson PG, Johnson NE, Butterfield RJ, Menafra R *et al* (2021) p53 convergently activates DUX/DUX4 in embryonic stem cells and in facioscapulohumeral muscular dystrophy cell models. *Nat Genet* 53: 1207 – 1220

Hendrickson PG, Doráis JA, Grow EJ, Whiddon JL, Lim JW, Wike CL, Weaver BD, Pflueger C, Emery BR, Wilcox AL *et al* (2017) Conserved roles of mouse DUX and human DUX4 in activating cleavage-stage genes and MERVL/HERVL retrotransposons. *Nat Genet* 49: 925 – 934

Hong AW, Meng Z, Yuan H, Plouffe SW, Moon S, Jho E, Guan K, Kim W, Jho E, Guan K-L (2017) Osmotic stress-induced phosphorylation by NLK at Ser128 activates YAP. *EMBO Rep* 18: 72 – 86

Ishiuchi T, Enriquez-Gasca R, Mizutani E, Bošković A, Ziegler-Birling C, Rodriguez-Terrones D, Wakayama T, Vaquerizas JM, Torres-Padilla ME (2015) Early embryonic-like cells are induced by downregulating replication-dependent chromatin assembly. *Nat Struct Mol Biol* 22: 662 – 671

Iturbide A, Torres-Padilla M (2020) A cell in hand is worth two in the embryo: recent advances in 2-cell like cell reprogramming. *Curr Opin Genet Dev* 64: 26 – 30

Iturbide A, Ruiz Tejeda Segura ML, Noll C, Schorpp K, Rothenaigner I, Ruiz-Morales ER, Lubatti G, Agami A, Hadian K, Scialdone A *et al* (2021) Retinoic acid signaling is critical during the totipotency window in early mammalian development. *Nat Struct Mol Biol* 28: 521 – 532

Khavari A, Ehrlicher AJ (2019) Nuclei deformation reveals pressure distributions in 3D cell clusters. *PloS One* 14: 1 – 13

Kumar A, Mazzanti M, Mistrik M, Kosar M, Beznoussenko GV, Mironov AA, Garrè M, Parazzoli D, Shivashankar GV, Scita G *et al* (2014) ATR mediates a checkpoint at the nuclear envelope in response to mechanical stress. *Cell* 158: 633 – 646

Le HQ, Ghatak S, Yeung C-YC, Tellkamp F, Günschmann C, Dieterich C, Yeroslaviz A, Habermann B, Pombo A, Niessen CM *et al* (2016) Mechanical regulation of transcription controls Polycomb-mediated gene silencing during lineage commitment. *Nat Cell Biol* 18: 864 – 875

Macfarlan TS, Gifford WD, Agarwal S, Driscoll S, Lettieri K, Wang J, Andrews SE, Franco L, Rosenfeld MG, Ren B *et al* (2011) Endogenous retroviruses and neighboring genes are coordinately repressed by LSD1/KDM1A. *Genes Dev* 4: 594 – 607

Macfarlan TS, Gifford WD, Driscoll S, Lettieri K, Rowe HM, Bonanomi D, Firth A, Singer O, Trono D, Pfaff SL (2012) Embryonic stem cell potency fluctuates with endogenous retrovirus activity. *Nature* 487: 2 – 10

Malik V, Wang J (2022) Pursuing totipotency: authentic totipotent stem cells in culture. *Trends Genet* 38: 632 – 636

Miroshnikova YA, Le HQ, Schneider D, Thalheim T, Rübsam M, Bremicker N, Polleux J, Kamprad N, Tarantola M, Wang I *et al* (2018) Adhesion forces and cortical tension couple cell proliferation and differentiation to drive epidermal stratification. *Nat Cell Biol* 20: 69 – 80

Nakatani T, Lin J, Ji F, Ettinger A, Pontabry J, Tokoro M, Altamirano-Pacheco L, Fiorentino J, Mahammadov E, Hatano Y *et al* (2022) DNA replication fork speed underlies cell fate changes and promotes reprogramming. *Nat Genet* 54: 318 – 327

Nava MM, Miroshnikova YA, Biggs LC, Whitefield DB, Metge F, Boucas J, Vihinen H, Jokitalo E, Li X, García Arcos JM *et al* (2020) Heterochromatin-driven nuclear softening protects the genome against mechanical stress-induced damage. *Cell* 181: 800 – 817.e22

Peña-Oyarzun D, Troncoso R, Kretschmar C, Hernando C, Budini M, Morselli E, Lavandero S, Criollo A (2017) Hyperosmotic stress stimulates autophagy via polycystin-2. *Oncotarget* 8: 55984 – 55997

Riveiro AR, Brickman JM (2020) From pluripotency to totipotency : an experimentalist's guide to cellular potency. *Development* 147: dev189845

Rodriguez-Terrones D, Gaume X, Ishiuchi T, Weiss A, Kopp A, Kruse K, Penning A, Vaquerizas JM, Brino L, Torres-Padilla ME (2018) A molecular roadmap for the emergence of early-embryonic-like cells in culture. *Nat Genet* 50: 106 – 119

Rodriguez-Terrones D, Hartleben G, Gaume X, Eid A, Guthmann M, Iturbide A, Torres-Padilla M (2020) A distinct metabolic state arises during the emergence of 2-cell-like cells. *EMBO Rep* 21: e48354

Salehi F, Behboudi H, Kavoosi G, Ardestani SK (2018) Oxidative DNA damage induced by ROS-modulating agents with the ability to target DNA: a comparison of the biological characteristics of citrus pectin and apple pectin. *Sci Rep* 8: 13902

Shah P, Hobson CM, Cheng S, Colville MJ, Paszek MJ, Superfine R, Lammerding J (2021) Nuclear deformation causes DNA damage by increasing replication stress. *Curr Biol* 31: 753 – 765.e6

Shen H, Yang M, Li S, Zhang J, Peng B, Wang C, Chang Z, Ong J, Du P (2021) Mouse totipotent stem cells captured and maintained through spliceosomal repression. *Cell* 184: 2843 – 2859.e20

Srinivas US, Tan BWQ, Vellayappan BA, Jeyasekharan AD (2019) ROS and the DNA damage response in cancer. *Redox Biol* 25: 101084

Srivastava LK, Ju Z, Ghagre A, Ehrlicher AJ (2021) Spatial distribution of Lamin A/C determines nuclear stiffness and stress-mediated deformation. *J Cell Sci* 134: jcs248559

Storm MP, Kumpfmueller B, Bone HK, Buchholz M, Sanchez Ripoll Y, Chaudhuri JB, Niwa H, Tosh D, Welham MJ (2014) Zscan4 is regulated by PI3-kinase and DNA-damaging agents and directly interacts with the transcriptional repressors LSD1 and CtBP2 in mouse embryonic stem cells. *PloS One* 9: e89821

Tagliaferri D, Mazzone P, Noviello TMR, Addeo M, Angrisano T, Del Vecchio L, Visconte F, Ruggieri V, Russi S, Caivano A *et al* (2020) Retinoic acid induces embryonic stem cells (ESCs) transition to 2 cell-like state through a coordinated expression of dux and Duxbl1. *Front Cell Dev Biol* 7: 385

Taïeb HM, Garske DS, Contzen J, Gossen M, Bertinetti L, Robinson T, Cipitria A (2021) Osmotic pressure modulates single cell cycle dynamics inducing reversible growth arrest and reactivation of human metastatic cells. *Sci Rep* 11: 13455

Uhlik MT, Abell AN, Johnson NL, Sun W, Cuevas BD, Lobel-Rice KE, Horne EA, Dell'Acqua ML, Johnson GL (2003) Rac-MEKK3-MKK3 scaffolding for p38 MAPK activation during hyperosmotic shock. *Nat Cell Biol* 5: 1104 – 1110

Wang F, Kooistra M, Lee M, Liu L, Baltz JM (2011) Mouse embryos stressed by physiological levels of osmolarity become arrested in the late 2-cell stage before entry into M phase. *Biol Reprod* 713: 702 – 713

Wang Y, Na Q, Li X, Tee WW, Wu B, Bao S (2021) Retinoic acid induces NELFA-mediated 2C-like state of mouse embryonic stem cells associates with epigenetic modifications and metabolic processes in chemically defined media. *Cell Prolif* 54: e13049

Watanabe K, Morishita K, Zhou X, Shiizaki S, Uchiyama Y, Koike M, Naguro I, Ichijo H (2021) Cells recognize osmotic stress through liquid-liquid phase separation lubricated with poly (ADP-ribose). *Nat Commun* 12: 1353

Willis J, Patel Y, Lentz BL, Yan S (2013) APE2 is required for ATR-Chk1 checkpoint activation in response to oxidative stress. *Proc Natl Acad Sci USA* 110: 10592 – 10597

Wu K, Liu H, Wang Y, He J, Xu S, Chen Y, Kuang J, Liu J, Guo L, Li D *et al* (2020) SETDB1-mediated cell fate transition between 2C-like and pluripotent states. *Cell Rep* 30: 25 – 36.e6

Yang M, Yu H, Yu X, Liang S, Hu Y, Luo Y, Izsvák Z, Sun C, Wang J (2022) Chemical-induced chromatin remodeling reprograms mouse ESCs to totipotent-like stem cells. *Cell Stem Cell* 29: 400 – 418.e13

Zafarullah M, Li WQ, Sylvester J, Ahmad M (2003) Molecular mechanisms of N-acetylcysteine actions. *Cell Mol Life Sci* 60: 6 – 20

Zhang Z, Dmitrieva NI, Park JH, Levine RL, Burg MB (2004) High urea and NaCl carbonylate in renal cells in culture and in vivo, and high urea causes 8-oxoguanine lesions in their DNA. *Proc Natl Acad Sci USA* 101: 9491 – 9496

Zhang JY, Diao YF, Kim HR, Jin D (2012) Inhibition of endoplasmic reticulum stress improves mouse embryo development. *PloS One* 7: e40433

Zhang C, Yan YL, Hao J, Wang Y (2019) Cellular redox state as a critical factor in initiating early embryonic-like program in embryonic stem cells. *Cell Discov* 5: 59

Zhu Y, Cheng C, Chen L, Zhang L, Pan H, Hou L, Sun Z, Zhang L, Fu X, Chan KY *et al* (2021) Cell cycle heterogeneity directs spontaneous 2C state entry and exit in mouse embryonic stem cells. *Stem Cell Reports* 16: 2659 – 2673

Expanded View Figures

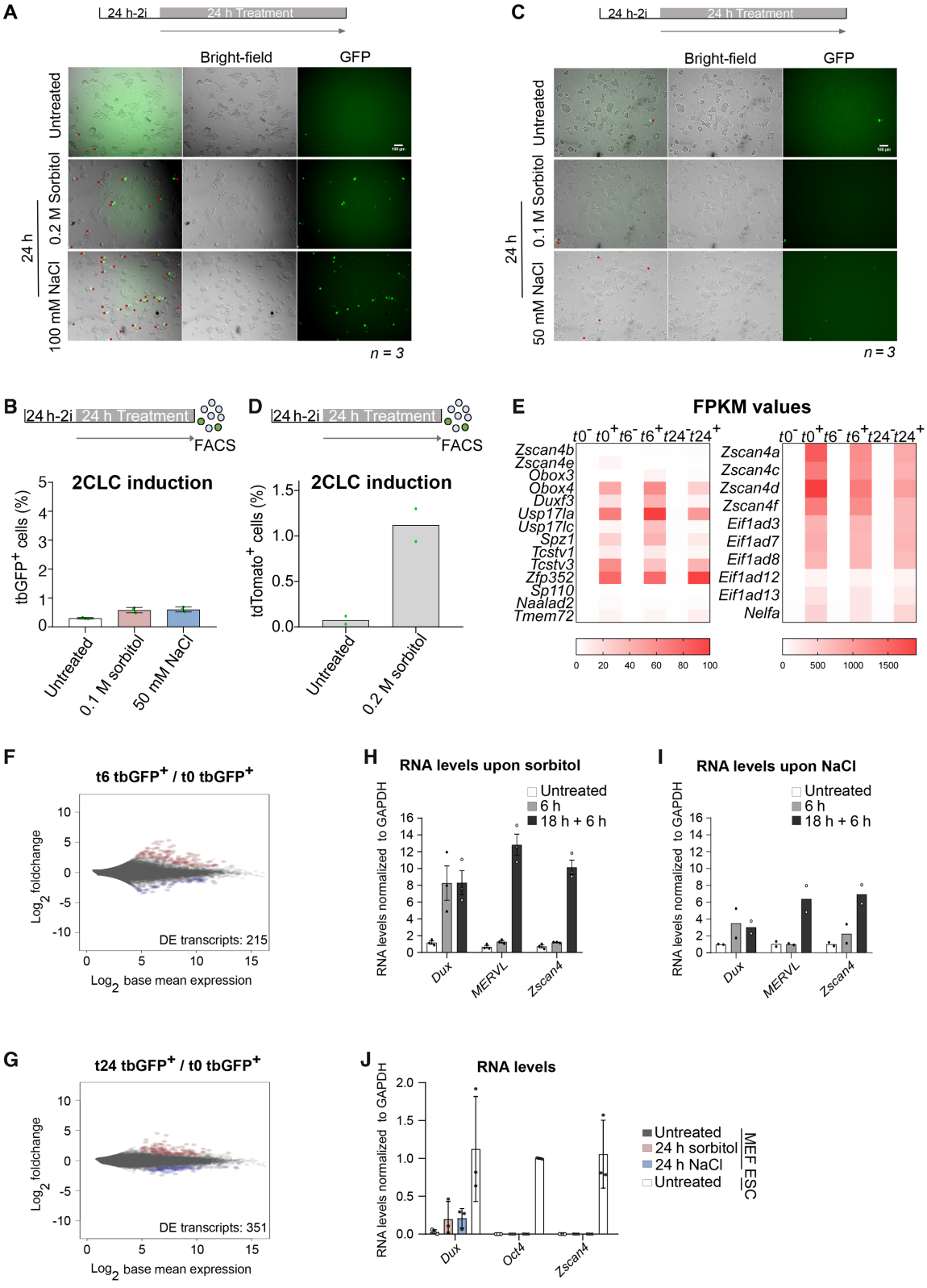

Figure EV1.

Figure EV1. Hyperosmotic stress induces 2CLCs.

A Representative images showing bright-field and GFP fluorescence from ESCs incubated for 24 h with indicated hyperosmotic treatment. Red arrows indicate tbGFP-positive 2CLCs. Scale bar: 100 μm.

B Percentage of 2CLCs obtained by FACS after the indicated sorbitol or NaCl treatments for 24 h. Shown are the mean from two replicates. Individual dots indicate measurement of an independent biological replicate by FACS.

C Representative image showing bright-field and GFP fluorescence from ESCs incubated for 24 h with the indicated hyperosmotic treatment. Red arrows indicate tbGFP-positive 2CLCs. Scale bar: 100 μm.

D Percentage of 2CLCs obtained by FACS after the indicated 0.2 M sorbitol treatment for 24 h. Shown are the mean from two replicates. Individual dots indicate measurement of an independent biological replicate by FACS.

E Heatmap depicting FPKM values of the 25 selected 2CLC markers from Fig 1G for all RNA-sequencing conditions. All genes displayed significative differential expression at t0, t6 and t24 sorbitol treatment in $tbGFP^+$ cells compared to $tbGFP^-$ cells of related time point ($P.adj < 0.01$).

F, G MA plots displaying differentially expressed genes in $tbGFP^+$ from t6 compared to t0 or t24 compared to t0. Significantly DE genes are highlighted in red for up-regulated transcripts and blue for downregulated transcripts ($P.adj < 0.05$; $Log_2FoldChange(tbGFP^+/tbGFP^-) > 1$ or -1).

H, I RT-qPCR analysis of the indicated genes in ESC cultures treated with sorbitol or NaCl for the indicated time. Shown are the mean ± s.d. of three independent replicates for (G) or the mean of two independent replicates for H. Individual dots indicate fold-change measurement for an independent biological replicate by qPCR.

J RT-qPCR of the indicated genes in MEF control (untreated) and treated with sorbitol or NaCl for 24 h and compared with untreated ESCs. *Oct4* is shown as comparison of a gene strongly and specifically expressed in ESCs. Shown are the mean ± s.d. of three independent replicates.

Source data are available online for this figure.

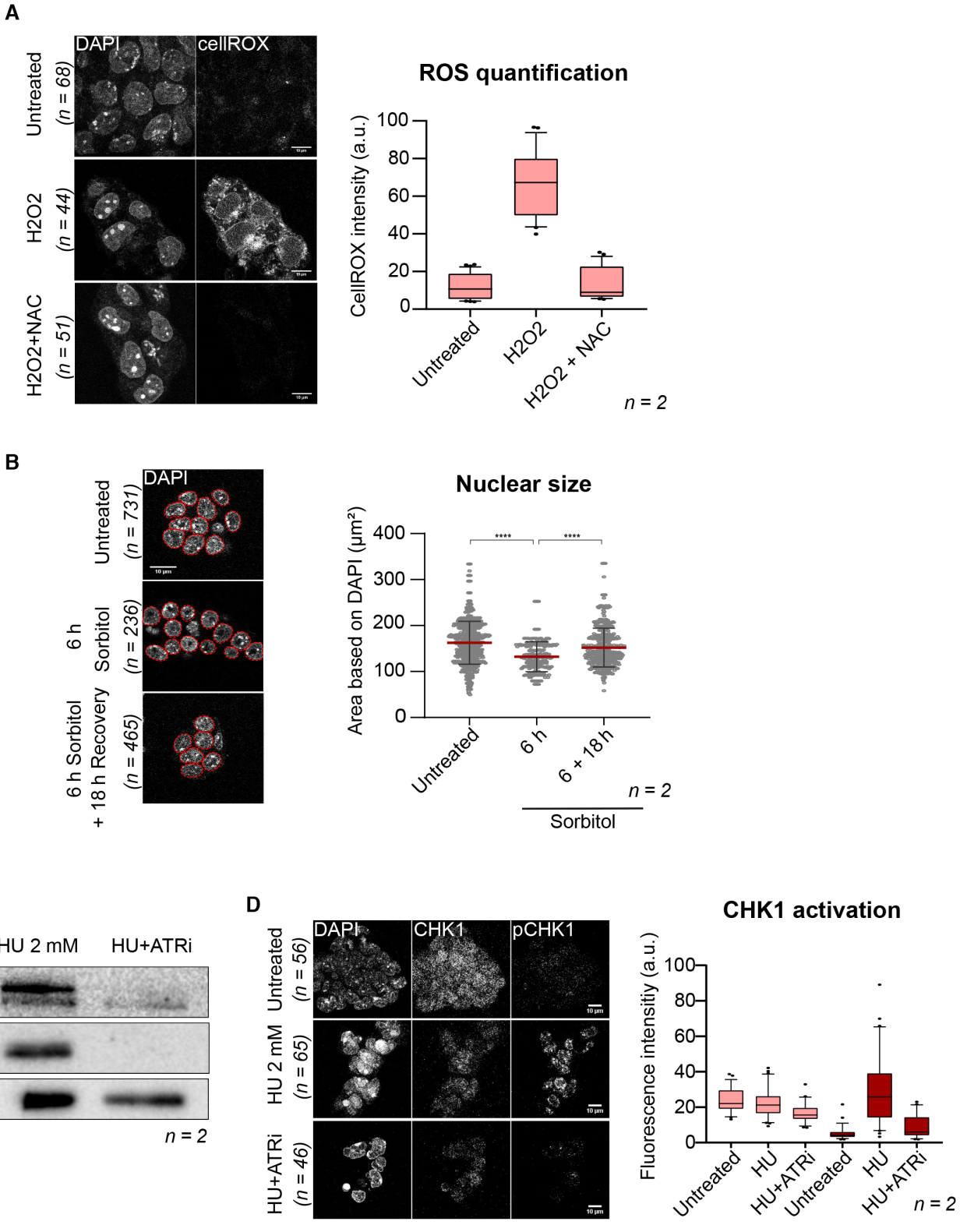
A
DAPI
cellROX
Untreated (n = 68)
H2O2 (n = 44)
H2O2+NAC (n = 51)
ROS quantification
CellROX intensity (a.u.)
100
80
60
40
20
0
Untreated
H2O2
H2O2 + NAC
n = 2
B
DAPI
Untreated (n = 731)
6 h Sorbitol (n = 236)
6 h Sorbitol + 18 h Recovery (n = 465)
Nuclear size
Area based on DAPI (µm²)
400
300
200
100
0
****
****
Untreated
6 h
6 + 18 h
n = 2
Sorbitol
C
HU 2 mM
HU+ATRi
pATR
pCHK1
GAPDH
n = 2
D
DAPI
CHK1
pCHK1
Untreated (n = 56)
HU 2 mM (n = 65)
HU+ATRi (n = 46)
CHK1 activation
Fluorescence intensity (a.u.)
100
80
60
40
20
0
Untreated
HU
HU+ATRi
Untreated
HU
HU+ATRi
n = 2

Figure EV2.

Figure EV2. Hyperosmotic-mediated 2CLC induction is mediated through ROS generation and ATR activation.

A (Left) Representative single confocal z-sections of CellROX-DeepRed fluorescence of ESCs treated with either hydrogen-peroxide (H_2O_2) with or without addition of the NAC ROS scavenger from two biological replicates. Scale bar: 10 μm. (Right) Boxplots showing quantification of CellROX-DeepRed fluorescence intensity from single z-sections. Boxes indicate the range between the first and third quartile, the line indicates the median and the whiskers display the spread from 5 to 95% of the data. Two-tailed Mann–Whitney tests were performed. A total of 68, 44, and 51 nuclei were quantified in untreated, H2O2, H202 + NAC, respectively.

B (Left) DAPI signal of representative single-section of ESCs treated with 0.2 M sorbitol for the indicated time from two biological replicates. Nuclei segmentation is shown in red. Scale bar: 10 μm. (Right) The plot displays median (red line) area ± s.d. of nuclear area as determined by DAPI fluorescence. Each dot represents a single nucleus from 2 biological replicates. Two-tail Mann–Whitney tests were performed. A total of 731, 236, and 465 nuclei were quantified in untreated, 6 h, 6 + 18 h sorbitol, respectively.

C Western blot analysis for the indicated antibodies in ESCs treated with hydroxy-urea (HU) with or without the ATR inhibitor. Shown is one representative image from two independent replicates. p, phosphorylated.

D (Left) Representative single confocal z-section of immunofluorescence for CHK1 and phosphoCHK1 (pCHK1) of ESCs treated with HU with or without ATR inhibitor from two biological replicates. Scale bar: 10 μm. (Right) Quantification of immunofluorescence intensities from single z-sections. A total of 56, 65, and 46 nuclei were quantified in untreated, 2 mM HU, 2 mM HU + ATRi, respectively. Boxes indicate the range between the first and third quartile, the line indicates the median and the whiskers display the spread from 5 to 95% of the data.

Data information: Stars indicate significant differences obtained using indicated statistical tests with *$P < 0.05$; **$P < 0.01$; ***$P < 0.001$; ****$P < 0.0001$.
Source data are available online for this figure.